

Coarse-grained Modeling and Simulation of Actin Filament Behavior Based on Brownian Dynamics Method

Yoshitaka Shimada^{*†}, Taiji Adachi^{*†‡}, Yasuhiro Inoue^{*†} and Masaki Hojo^{*}

Abstract: The actin filament, which is the most abundant component of the cytoskeleton, plays important roles in fundamental cellular activities such as shape determination, cell motility, and mechanosensing. In each activity, the actin filament dynamically changes its structure by polymerization, depolymerization, and severing. These phenomena occur on the scales ranging from the dynamics of actin molecules to filament structural changes with its deformation due to the various forces, for example, by the membrane and solvent. To better understand the actin filament dynamics, it is important to focus on these scales and develop its mathematical model. Thus, the objectives of this study were to model and simulate actin filament polymerization, depolymerization, and severing based on the Brownian dynamics method. In the model, the actin monomers and the solvent were considered as globular particles and a continuum, respectively. The motion of the actin molecules was assumed to follow the Langevin equation. The polymerization, which increases the filament length, was determined by the distance between the center of the actin particle at the barbed end and actin particles in the solvent. The depolymerization, which decreases the filament length, was modeled such that the number of dissociation particles from the filament end per unit time was constant. In addition, the filament severing, in which one filament divides into two, was modeled to occur at an equal rate along the filament. Then, we sim-

ulated the actin filament dynamics using the developed model, and analyzed the filament elongation rate, its turnover, and the effects of filament severing on the polymerization and depolymerization. Results indicated that the model reproduced the linear dependence of the filament elongation on time, filament turnover process by polymerization and depolymerization, and acceleration of the polymerization and depolymerization by severing, which qualitatively agreed with those observed in experiments.

Keyword: Actin filament, Computational biomechanics, Brownian dynamics method, Coarse-grained modeling, Multiscale modeling and simulation, Cell biology

1 Introduction

The actin filament, which is a double-helical polymeric filament consisting of actin monomers, plays important roles in fundamental cellular activities such as shape determination, cell motility, and mechanosensing (1-3). In each activity, the actin filament dynamically changes its structure by polymerization, depolymerization, and severing (4, 5). Because of the polarity of the actin molecule, the two ends of the polymerized filament, termed as the barbed (plus) and pointed (minus) ends (6), have different properties. The actin filament elongates by the polymerization of actin monomers at the filament ends. Polymerization occurs mainly at the barbed end (7), the rate of which is enhanced by actin-related proteins such as formin (8) and Arp2/3 complex (9). The depolymerization induced by ADF/cofilin (10) is a dissociation process of actin molecules from the filament end, and plays important roles in the recycling of actin molecules and in preventing the

^{*} Department of Mechanical Engineering and Science, Kyoto University

[†] Computational Cell Biomechanics Team, VCAD System Research Program, RIKEN

[‡] Corresponding author. Department of Mechanical Engineering and Science, Kyoto University, Yoshida-Honmachi, Sakyo, Kyoto 606-8501, Japan. E-mail: adachi@me.kyoto-u.ac.jp

depletion of actin monomers (6). Severing shortens its average length and results in an increase in the number of filaments, which is regulated by ADF/cofilin and gelsolin (4, 11). Thus, these three are fundamental phenomena governing actin filament dynamics.

The actin filament dynamics occur on various spatial and temporal scales ranging from the atomistic structure dynamics of the actin molecule to the cellular system dynamics such as motility and division (12). The atomistic structures of the actin molecule at angstrom scale change its conformation in picoseconds (13). Actin molecules, whose diameters are of nanometer scale (14), are moved in the cytoplasm by random forces at nanosecond scale. The actin filament, whose length scale ranges from nanometer to micrometer, changes its structures by polymerization, depolymerization, and severing on a temporal scale from microseconds to seconds (15). Actin filaments interact with other filaments through crosslinking and bundling to form the network structures (16), and the extension of network structures by polymerization causes, for example, cellular motility whose velocity is at the scale of micrometer per second (17). Thus, the actin filament dynamics exhibit characteristic structure-function relationships in various spatial and temporal scales.

To investigate the filament behaviors on various spatial and temporal scales, developing mathematical models of actin filament dynamics suitable for these scales is required. Many mathematical models of actin filament dynamics have been developed. For example, on the atomistic structure dynamics scale, molecular dynamics simulations on a repeat unit of filamentous actin molecules that bind ATP and ADP have characterized the significant effects of the DNase I-binding loop conformation on the structural and mechanical properties of the actin filament (13). On the scales ranging from molecular to filament structure, a coarsegrained model of the actin filament has been developed from atomic-scale simulations to calculate its stiffness (18). On the filament dynamics scale, to investigate the elastic deformation modes of the actin filament, a molecular structure of the filament has been modeled as

an assemblage of substructures (19). On the scale of filament structural changes, filament elongation has been described using a stochastic model, and the enhancement of polymerization by severing has been simulated (15). On the scales ranging from the filament structural changes to cellular motility, a set of partial differential equations for diffusion and reactions of the sequestered actin complexes, nucleation, polymerization, depolymerization, and capping has been developed to obtain the relationship between the protrusion velocity and the number of filament barbed ends (20).

Moreover, polymerization, depolymerization and severing, which constitute the actin filament dynamics, occur on the scales ranging from the dynamics of actin molecules to filament structural changes with its deformation due to the various forces, for example by the membrane and solvent. Therefore, it is important to develop a new mathematical model that captures these scales, in order to better understand actin filament dynamics with its deformation. The actin filament dynamics deal with numerous interactions among actin filamentous molecules, monomers, and solvent molecules including water in the cytoplasm. Thus, it is preferable to coarse-grain these molecules, in the development of mathematical model describing the spatial and temporal scales, using the Brownian dynamics method (21, 22).

The purpose of this study is to develop mathematical model of actin filament dynamics describing spatial and temporal scales ranging from the actin molecular dynamics to filament structural changes, focusing on the polymerization, depolymerization, and severing. To simulate the filament dynamics over the spatial and temporal scales, the actin molecules, filament structures, solvent, and filament structural changes are coarse-grained and modeled as follows. 1) The actin molecules are considered as globules with mass and size. 2) The actin filament is described as a linear chain of globular particles with spring bonds. 3) A solvent model is also described using the Brownian dynamics method, in which the solvent for actin molecules is considered as continuum, and the mechanical effects from the behavior of solutes

are assumed to be from random and dissipative forces. And, 4) the filament structural changes are modeled based on the polymerization distance, depolymerization rate, and severing rate. Finally, we simulate the actin filament dynamics and analyze the filament elongation rate, its turnover, and the effects of filament severing on the polymerization and depolymerization.

2 Description of model

2.1 Brownian dynamics method

In this study, atomistic structures of the actin molecule are coarse-grained as globular particles with a diameter $l_0 = 5.4$ nm and the solvent as a continuum, in which the rotation of the coarse-grained actin particle in the solvent is not considered. Thus, the motion of the particle, existing at position (\mathbf{r}) with a mass (m), follows the Langevin equation,

$$m \frac{d\mathbf{v}}{dt} = \mathbf{f} - \gamma \mathbf{v} + \mathbf{f}^B, \quad (1)$$

where \mathbf{v} is the particle velocity in the solvent, \mathbf{f} and \mathbf{f}^B are the external and random forces acting on the particle, and γ is a friction constant. The friction constant γ is expressed by

$$\gamma = \frac{k_B T}{D}, \quad (2)$$

where D is a diffusion coefficient of the actin particle in the solvent, k_B is the Boltzmann constant, and T is temperature. The external force \mathbf{f} is a conservative force determined from the potential acting on the actin particle. Assuming an equilibrium state, the random force will have no time correlation, its time mean becomes zero, and its variance becomes $2\gamma k_B T$. Thus, the random force \mathbf{f}^B acting on the particle can be expressed by

$$\langle f_i^B(t) \rangle = 0 \quad (i = 1, 2, 3), \quad (3)$$

$$\langle \{f_i^B(t)\}^2 \rangle = 2\gamma k_B T, \quad (4)$$

where the bracket $\langle \rangle$ denotes the time average.

2.2 Actin filament dynamics model

To eliminate the geometric complexity of the double-helix structure, we approximate the actin filament as a linear chain model. Filamentous actin particles are bonded linearly, as shown in Fig. 1A, in the elongation direction by linear springs with a constant K_{tensile} [pN/nm] and equilibration distance l_{eq} [nm]. To match the filamentous particle density along the length of our linear model with that of the double-helix structure, in this study, l_{eq} is set as 2.7 nm ($= l_0/2$) (20). In the bending direction, interparticles are bonded by a linear bending spring with a constant K_{bend} [pN·nm²], as shown in Fig. 1B. The length of the actin filament L_{filament} [nm] can be expressed by

$$L_{\text{filament}} = N_{\text{FActin}} l_{\text{eq}}, \quad (5)$$

where N_{FActin} [particles] is the number of filamentous actin particles in a single filament. In this study, we define that the filament consists of more than two particles.

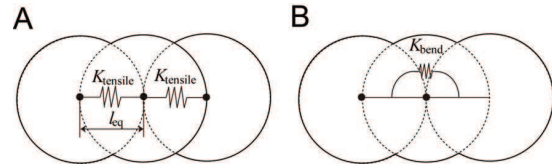


Figure 1: Schematics of actin filament model. (A) Filamentous particles are bonded by linear springs with a constant K_{tensile} and equilibrium distance l_{eq} . (B) In the bending direction, interparticles are bonded by a linear bending spring with a constant K_{bend} .

Figure 2 shows the actin dynamics model. The actin filament has two polarized ends, those are distinguished by the net polymerization/depolymerization rates. In this study, focusing on the net rates, each ends are individually modeled as the polymerizing barbed end and depolymerizing pointed end. Severing is modeled to occur at inter-particles, resulting in an increase in the number of filaments by one for every severing.

2.3 Mathematical modeling of polymerization

Polymerization by bonding an actin monomer to the barbed end is a fundamental process of fila-

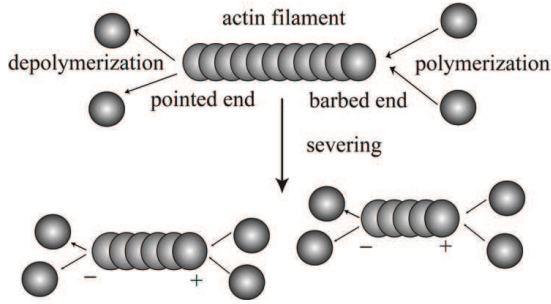


Figure 2: Schematic of actin filament dynamics model. We modeled that polymerization occurs only at the barbed end, depolymerization at the pointed end, and severing at interparticles, resulting in an increase in the number of filaments.

ment elongation. In this study, we coarse-grain the actin molecules as particles, and neglect the chemical reactions at the molecular level. We, therefore, assume that the polymerization simply depends on the distance between the filament barbed end and an actin particle in the solvent. We set an orthogonal coordinate system ($O-x_1, x_2, x_3$) ($x_1 \geq 0$) whose origin is set at the center of the actin particle at the barbed end, and denote its base vectors by $(\mathbf{e}_1, \mathbf{e}_2, \mathbf{e}_3)$, where the elongation direction is set along the x_1 axis, as shown in Fig. 3A. To express asymmetric accessibility of the particle to the barbed end due to the interference with the filament, we set the offset $r_{\text{off}} = l_0$ for the polymerization center from the barbed end, as shown as Fig. 3B, where l_0 is the particle diameter. Thus, the polymerization occurs when the distance satisfies the condition of $(r_1 - l_0)^2 + r_2^2 + r_3^2 < \Delta_p^2$, where $\mathbf{r}(r_1, r_2, r_3)$ is the position of the actin particle and Δ_p is the polymerization distance. Then, we model the polymerization by bonding the particles to the plus end using the spring at the polymerization distance Δ_p , and set Δ_p empirically as 2.7 nm ($= l_0/2$) in this study.

2.4 Mathematical modeling of depolymerization

Depolymerization is a phenomenon in which an actin molecule dissociates from the pointed end

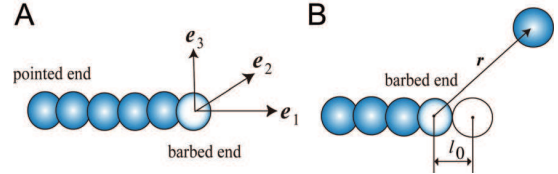


Figure 3: Schematics of polymerization model. (A) Orthogonal coordinate system whose origin is set at the center of the actin particle at the barbed end, and its base vectors $(\mathbf{e}_1, \mathbf{e}_2, \mathbf{e}_3)$, where the elongation direction is set along the x_1 axis. (B) Distance between the barbed end particle and the particle in the solvent.

and results in the shortening of the filament length (23). Experiments on depolymerization have revealed that the dissociation rate of actin molecules from the pointed end per unit time is constant (6). Thus, the rate of change in the filament length L_{filament} can be expressed as

$$\frac{dL_{\text{filament}}}{dt} = l_{\text{eq}} \frac{dN_{\text{Factin}}}{dt} = -l_{\text{eq}} k_d, \quad (6)$$

where the depolymerization rate k_d [particles/ μs] is the dissociation rate of actin particles per unit time. In this study, to prevent the filament from disappearing, we assume that the depolymerization occurs when the filament consists of at least two particles.

2.5 Mathematical modeling of severing

Severing an existing filament into smaller ones decreases its average length and increases its number. We assume that the severing at the interparticle occurs at an equal rate along the filament (15, 24, 25). Additionally, because we defined that the filament consists of more than two particles, we assumed that the severing occurs except for the interparticles at both ends. Thus, the severing rate at the inter-particle, k_{sev} [$1/\mu\text{s}$], provides the severing rate of a single filament, $k_{\text{sev - filament}}$ [$1/\mu\text{s}$], which is described as

$$k_{\text{sev - filament}} = k_{\text{sev}} (N_{\text{Factin}} - 3) \quad (7)$$

that linearly depends on the filament length.

3 Numerical method

In this study, we assume that the actin filament dynamics depend on a diffusion-limited reaction (26), and the most dominant force for the motion of an actin particle is the random force. Thus, assuming that the attractive force is negligibly small, we use the repulsive term of the 6/12 Lennard Jones potential acting on the particles. Here, we explain a method of numerical integration of the Langevin equation, and set a time step, a potential coefficient, and spring constants.

3.1 Numerical integration method

The motion of the actin particle follows the Langevin equation in Eq. 1 derived from Brownian dynamics. The relaxation time of the actin particle by the dissipative force in the solvent, which is defined as

$$\Delta t_r = \frac{m}{\gamma} = \frac{mD}{k_B T}, \quad (8)$$

can be estimated as $\Delta t_r = 0.17$ ps from the molecular weight of actin ~ 42000 (27) and Eq. 2. To simulate actin filament dynamics ranging over a temporal scale from nanoseconds to microseconds, it is preferable to use a time step Δt that is longer than the relaxation time Δt_r . Thus, the particle position \mathbf{r} can be expressed as

$$\mathbf{r}(t + \Delta t) = \mathbf{r}(t) + \frac{1}{\gamma} \mathbf{f}(t) \Delta t + \Delta \mathbf{r}^B, \quad (9)$$

$$\langle \Delta r_i^B \rangle = 0 \quad (i = 1, 2, 3), \quad (10)$$

$$\langle (\Delta r_i^B)^2 \rangle = \frac{2k_B T}{D}. \quad (11)$$

From Eqs. 10 and 11, $\Delta \mathbf{r}^B$ follows the normal distribution, $\rho_{\text{normal}}(\Delta r_i^B)$, expressed as

$$\rho_{\text{normal}}(\Delta r_i^B) = \left(\frac{\gamma}{4\pi k_B T} \right)^{1/2} \exp \left\{ -\frac{\gamma}{4\pi k_B T \Delta t} (\Delta r_i^B)^2 \right\}. \quad (12)$$

Following this normal distribution, $\Delta \mathbf{r}^B$ is given by

$$\Delta r_i^B = \left(-\frac{4k_B T}{D} \ln R_1 \right)^{1/2} \cos(2\pi R_2), \quad (13)$$

where R_1 and R_2 are independent random variables from the same rectangular density function on the interval (0,1) (28).

3.2 Time step

For the numerical integration of the Langevin equation in Eq. 9 with the conditions of Eqs. 10 and 11, the time step should be determined to satisfy the following inequalities: the time step Δt is longer than the relaxation time Δt_r , and the magnitude of the particle displacement $|\Delta \mathbf{r}|$ during the time step is much smaller than a specific length of the repulsive potential acting on the particles, in which the diameter of the particle l_0 is employed as the specific length.

The particle displacement by random forces \mathbf{f}^B during Δt satisfies equations:

$$\langle \Delta \mathbf{r}(t) \rangle = 0, \quad (14)$$

$$\langle \{ \Delta \mathbf{r}(t) \}^2 \rangle = 6D\Delta t, \quad (15)$$

that is, the particle displacement during Δt follows the normal distribution with the mean zero and the variance $\sigma^2 = 6D\Delta t$. To prevent numerical instability in integration, it is necessary for the particle displacement $|\Delta \mathbf{r}|$ during Δt to be smaller than the specific length of the repulsive potential that is the particle diameter, l_0 . Thus, the time step Δt is determined under the condition, $|\Delta \mathbf{r}| = 3\sigma = 0.27$ nm, which is much smaller than $l_0 = 5.4$ nm. Substituting $D = 10 \mu\text{m}^2/\text{s}$ (20, 29, 30, 31), $k_B T = 4.1$ pN·nm (14), and $|\Delta \mathbf{r}| = 0.27$ nm into Eqs. 2 and 15, we can obtain $\Delta t = 135$ ps, which is sufficiently longer than the relaxation time $\Delta t_r = 0.17$ ps, enabling us to follow the motion of the actin particle by solving Eq. 9 in every time step.

3.3 Potential coefficient

The repulsive potential Φ is expressed by

$$\Phi(|\mathbf{r}_i - \mathbf{r}_j|) = 4\varepsilon \left(\frac{l_0}{|\mathbf{r}_i - \mathbf{r}_j|} \right), \quad (16)$$

where ε is an energy coefficient, and $|\mathbf{r}_i - \mathbf{r}_j|$ is a distance between the i th and j th actin particles. We determine the coefficient ε to satisfy the condition that the interparticle distance never becomes much smaller than the diameter, l_0 , by the following procedures. As a function of the coefficient ε , we calculate the average distance,

$\langle |\mathbf{r}_i - \mathbf{r}_j| \rangle$, between two particles that approach each other under directed random force. To satisfy the condition $\langle |\mathbf{r}_i - \mathbf{r}_j| \rangle = l_0$, we determine the coefficient $\varepsilon = 2.0 \times 10^{-21} \text{ J}$.

3.4 Spring constants for filamentous actin particles

The tensile stiffness of a single actin filament with a length $L_{\text{exp}} = 1 \mu\text{m}$ has been experimentally estimated as $K_{\text{exp}} = 43.7 \text{ pN/nm}$ (32). By modeling the actin filament with double-helical structure as a series of linear springs, the spring equilibrium distance was set as 2.7 nm, as shown in Fig. 1A. Thus, the tensile spring constant K_{tensile} is determined as $K_{\text{tensile}} = K_{\text{exp}} \times (1 \mu\text{m} / 2.7 \text{ nm}) = 1.62 \times 10^4 \text{ pN/nm}$.

By assuming that the filament under the stretch is modeled as a homogeneous cylindrical structure with a cross-sectional area $A = \pi l_0^2 / 4$ and a length l_{eq} , Young's modulus $E = 1.91 \times 10^3 \text{ pN/nm}^2$ was obtained by

$$F = \frac{EA}{l_{\text{eq}}} \Delta l_{\text{eq}} = K_{\text{tensile}} \Delta l_{\text{eq}}, \quad (17)$$

where F is an acting axial force and Δl_{eq} is its extension.

In the bending of a cylindrical structure, the bending moment M is described as

$$M = EI\kappa = K_{\text{bend}}\kappa, \quad (18)$$

where I is the moment of inertia of the area given by $I = \pi l_0^4 / 64$, and κ is the curvature. Thus, from Eq. 18, the bending spring constant K_{bend} is obtained as $K_{\text{bend}} = 7.97 \times 10^4 \text{ pN}\cdot\text{nm}^2$. The orders of magnitude of E and $EI = K_{\text{bend}}$ agree with those obtained by previous experiments (33, 34).

The force and moment generated by the springs are described as the external force term in the Langevin equation, Eqs. 1 and 9, and the particle positions are calculated by integrating the equation. When the time step $\Delta t = 135 \text{ ps}$ is used, we find that these spring constants, K_{tensile} and K_{bend} , are too large to obtain the stable numerical integration of the Langevin equation. To avoid this numerical instability, we reduce the spring constants by 1/20 to $K_{\text{tensile}} = 8.10 \times 10^2 \text{ pN/nm}$ and

$K_{\text{bend}} = 3.99 \times 10^3 \text{ pN}\cdot\text{nm}^2$, which have negligible effect on the polymerization, depolymerization, and severing targeted in this study.

3.5 Simulation conditions

We use the periodic boundary condition in which calculation cell sizes are 300 nm in the x_1 direction and 100 nm in the x_2 and x_3 directions, as shown in Fig. 4. As an initial state, an actin filament consisting of 20 actin particles with 54 nm ($= 20l_{\text{eq}}$) length is arranged at the center of the cell, and 180 actin particles ($\sim 100 \mu\text{M}$) are randomly placed around the actin filament.

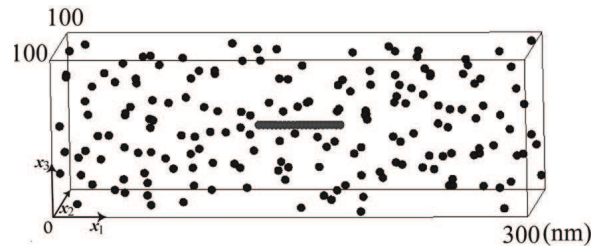


Figure 4: Snapshot of initial molecular configurations. The calculation cell sizes are 300 nm in the x_1 direction and 100 nm in the x_2 and x_3 directions. An actin filament is arranged at the center of the cell, and 180 actin particles ($\sim 100 \text{ M}$) are randomly placed around the actin filament.

4 Results

4.1 Filament elongation by polymerization

It has been reported that the elongation of an actin filament by polymerization has a linear dependence on time (6). To demonstrate this linearity, we simulated the actin filament elongation using the polymerization model developed in this study.

A change in the number of filamentous actin particles, N_{FActin} [particles], was calculated for $500 \mu\text{s}$ ($\sim 3.71 \times 10^6$ steps) from 10 different initial particle configurations, and Fig. 5 shows a snapshot of the filament in its elongation under the fluctuation. In Fig. 6, the change in the average number of filamentous actin particles N_{FActin} in time is plotted by solid circles, in which the error bars represent

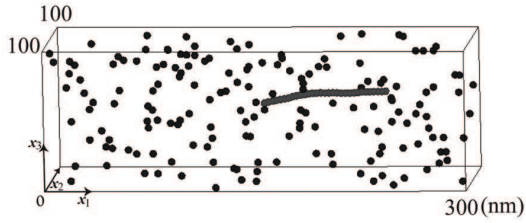


Figure 5: Snapshot of the filament under the fluctuations in elongation simulation at $t = 500\mu\text{s}$.

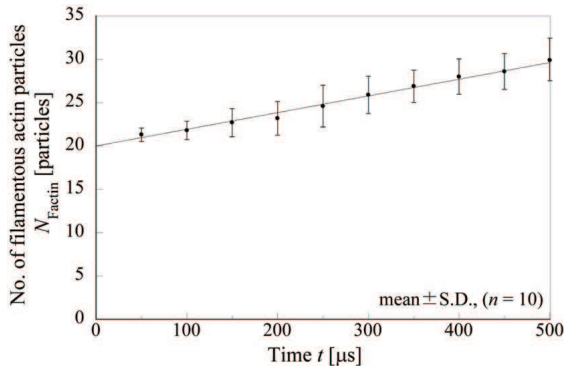


Figure 6: Change in number of filamentous particles in time. The solid circles indicate the simulated results, in which the error bars represent the standard deviation. The solid line describes the linear regression curve between N_{Factin} and t , which is obtained by the least-square method.

the standard deviation for 10 calculations. The solid line indicates the linear regression curve between N_{Factin} and t , which is obtained by the least-square method applied to the average values calculated at every $0.135\mu\text{s}$ (1×10^3 steps), that is,

$$N_{\text{Factin}}(t) = k_p t + N_{\text{Factin}}(0) = 1.93 \times 10^{-2} t + 20, \quad (19)$$

where k_p is the polymerization rate [particles/ μs]. The linearity between the filament elongation and time observed in the experiment was reproduced using the polymerization model proposed in this study.

The elongation rate in the case of an actin monomer concentration of $100\mu\text{M}$ was experimentally obtained as 1.16×10^{-3} molecules/ μs (6). Compared with this value, the gradient of Eq. 19 simulated in this study was larger by ~ 17

times. This difference might be due to the neglect of actin molecular polarity and the discrepancy of polymerization distance, Δ_p .

4.2 Actin filament turnover

Actin filaments undergo turnover, which is the exchange of actin molecules from existing filaments and the flux of molecules through the filament, by polymerization and depolymerization (23, 35-37). To demonstrate the turnover, we numerically investigated the relationship between the number of filamentous actin particles N_{Factin} [particles] and depolymerization rate k_d [particles/ μs], and the movement of the particle in the filament.

A change in the average number of filamentous actin particles N_{Factin} [particles] was calculated for $500\mu\text{s}$ ($\sim 3.71 \times 10^6$ steps) from 10 different initial particle configurations using 3 different depolymerization rates. The depolymerization rates were set as $k_d = 0.00$ [particles/ μs], in which depolymerization did not occur, $k_d = 1.93 \times 10^{-2}$ [particles/ μs], that was equal to the polymerization rate k_p obtained in this study, and $k_d = 3.86 \times 10^{-2}$ [particles/ μs], that was twofold the polymerization rate k_p .

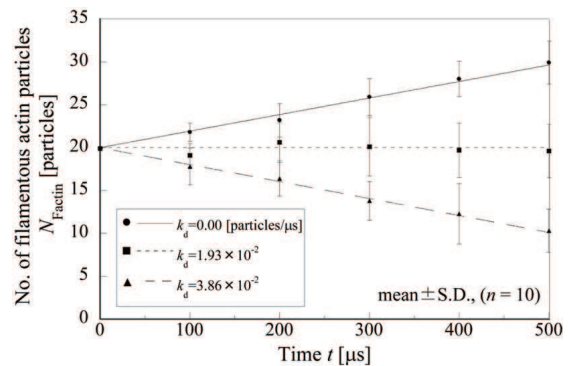


Figure 7: Change in number of filamentous particles in time. The solid circles, squares, and triangles indicate the simulated results for $k_d = 0.00$, 1.93×10^{-2} , and 3.86×10^{-2} particles/ μs , respectively, in which the error bars represent the standard deviation. The solid, dotted, and dashed lines describe the linear regression curve between N_{Factin} and t for $k_d = 0.00$, 1.93×10^{-2} , and 3.86×10^{-2} particles/ μs , respectively.

In Fig. 7, the changes in the average number of filamentous actin particles N_{FActin} in time are plotted by solid circles, squares, and triangles for $k_d = 0.00$, 1.93×10^{-2} , and 3.86×10^{-2} particles/ μs , respectively, in which the error bars represent the standard deviation. The lines indicate the linear regression curve between N_{FActin} and t , which were obtained by the least-square method applied to the average of the simulation results calculated at every $0.135 \mu\text{s}$ (1×10^3 steps):

$$N_{\text{FActin}}(t) = 1.93 \times 10^{-2}t + 20$$

$$(k_d = 0.00 \text{ particles}/\mu\text{s}), \quad (20)$$

$$N_{\text{FActin}}(t) = 20$$

$$(k_d = 1.93 \times 10^{-2} \text{ particles}/\mu\text{s}), \quad (21)$$

and

$$N_{\text{FActin}}(t) = -1.98 \times 10^{-2}t + 20$$

$$(k_d = 3.86 \times 10^{-2} \text{ particles}/\mu\text{s}). \quad (22)$$

For $k_d = 0.00$, because of no depolymerization, Eq. 20 is identical to Eq.19, and the increase in N_{FActin} has a linear dependence on time. For $k_d = 1.93 \times 10^{-2}$, the linear regression curve in Eq. 21 is equal to the initial condition (20 particles), because the depolymerization rate was set to be equal to the polymerization rate. For $k_d = 3.86 \times 10^{-2}$, N_{FActin} decreased because the depolymerization rate was higher than the polymerization rate. The magnitudes of dN_{FActin}/dt in Eqs. 20-22 agree well with the difference between k_p and k_d , that is, $k_p - k_d = 1.93 \times 10^{-2}$, 0.00 , and 1.93×10^{-2} , respectively. Thus, the results indicated that the change in the average number of filamentous actin particles N_{FActin} can be calculated using the difference between the polymerization and depolymerization rates.

To numerically observe the turnover process, the change in the number of filamentous actin particles N_{FActin} , the positions of the particle that was initially at the barbed-end, and the barbed-end particles are illustrated at every $13.5 \mu\text{s}$ (1×10^5 steps) in Fig. 8. The actin filament was schematically represented as a linear particle model. The movement of the initial barbed-end particle is

shown in green, and the barbed-end particles are in red.

Figure 8A ($k_d = 0.00$) shows that the position of the green particle (the initial barbed-end particle) remained at the 20th from the pointed end particle, while the red particle (the barbed-end particle) moved forward by polymerization. In Fig. 8B ($k_d = 1.93 \times 10^{-2}$), the position of the green particle moved toward the pointed end, while the average number of filamentous actin particles N_{FActin} stayed around 20, which was equal to that of the initial state. Thus, the result for $k_d = 1.93 \times 10^{-2}$ particles/ μs indicated the treadmilling phenomenon (23, 37). Figure 8C ($k_d = 3.86 \times 10^{-2}$) shows that the green particle moved toward the pointed end faster than that in $k_d = 1.93 \times 10^{-2}$ and the total number of filamentous actin particles decreased. From these three results, by using the polymerization and depolymerization models, the action the filament turnover process and treadmilling were reproduced.

4.3 Effect of severing on poly- and depolymerization

Because the actin filament changes its structure by polymerization, depolymerization and severing, we investigated the effects of severing on poly- and depolymerization using the model developed in this study.

Changes in the average numbers of filament N_F , filamentous actin particles N_{FActin} , polymerized actin particles N_p , and depolymerized actin N_d were calculated for $500 \mu\text{s}$ ($\sim 3.71 \times 10^6$ steps) from 10 different initial particle configurations. Assuming that the filament severing occurs statistically once every $500 \mu\text{s}$, the severing rate can be set as $k_{\text{sev}} = 1.18 \times 10^{-4}$ [$1/\mu\text{s}$] using Eq. 7. The depolymerization rate is set as $k_d = 1.93 \times 10^{-2}$ [particles/ μs], that is equal to the polymerization rate k_p obtained in this study. Figure 9 shows a snapshot of the filament after severing under the fluctuation. The changes in the average numbers of filament N_F and filamentous actin particles N_{FActin} are shown in Figs. 10A and 10B, respectively. Figure 10A indicates that the average number of filament N_F increases because of filament severing. Figure 10B shows that the number of

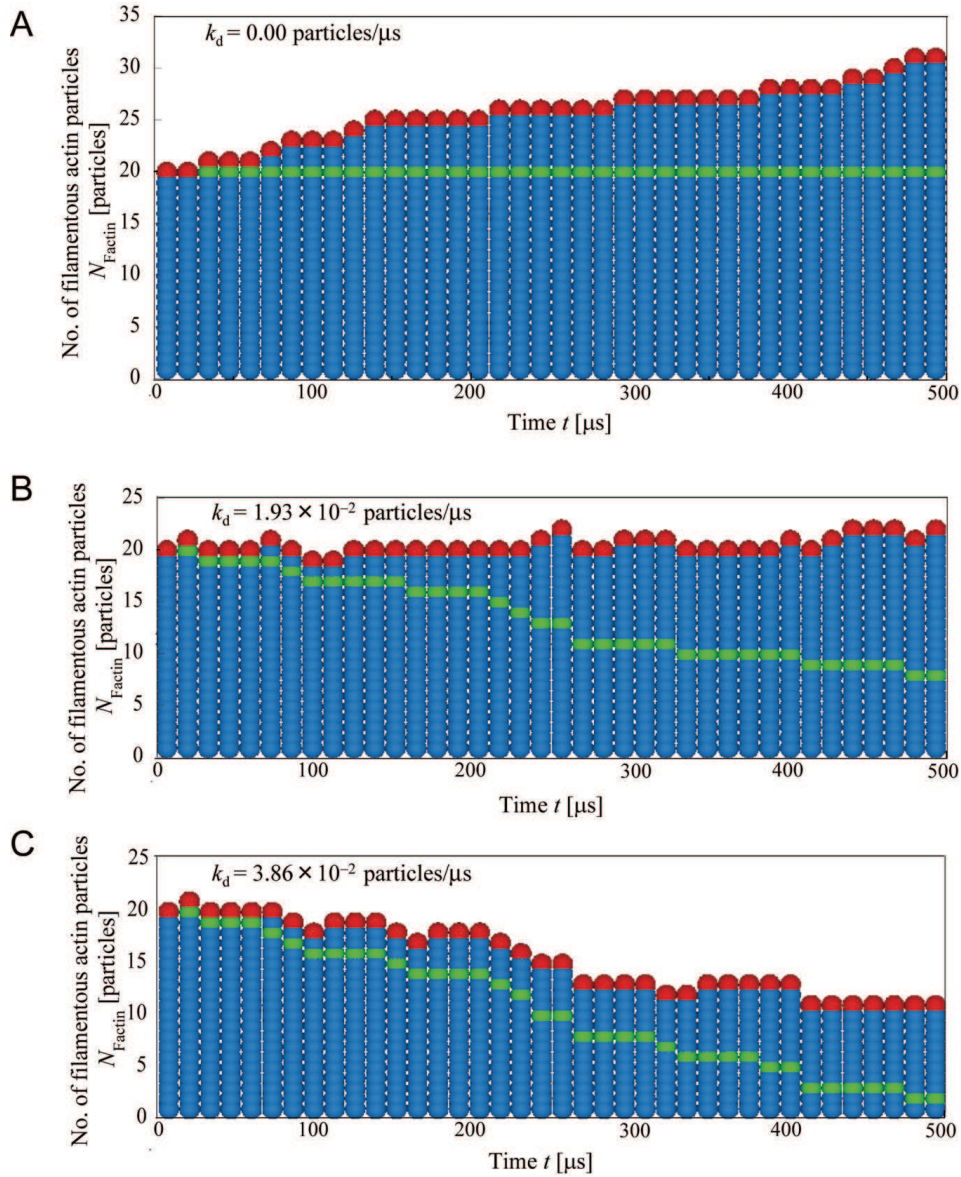


Figure 8: Change in number of filamentous actin particles N_{Factin} in time. The positions of the particle initially at the barbed end and the barbed end particles at every $13.5\mu\text{s}$ are illustrated for (A) $k_d = 0.00$, (B) 1.93×10^{-2} , and (C) 3.86×10^{-2} particles/ μs , respectively, as a case study. The movement of the initial barbed end particle is shown in green, and those of the barbed end particles are in red.

filamentous particles N_{Factin} is almost 20, which is equal to that of the initial state, because the depolymerization rate was set to be equal to the polymerization rate.

In Fig. 10C, the change in the number of polymerized actin particles N_p is shown, in which the solid line indicates the simulated result, and the

dotted line indicates the relation,

$$N_p(t) = k_p t = 1.93 \times 10^{-2} t, \quad (23)$$

which was obtained from Eq. 19 under the assumption of no severing. The change in the number of polymerized actin particles N_p is proportional to the number of filaments. Thus, considering the change in the number of filaments illus-

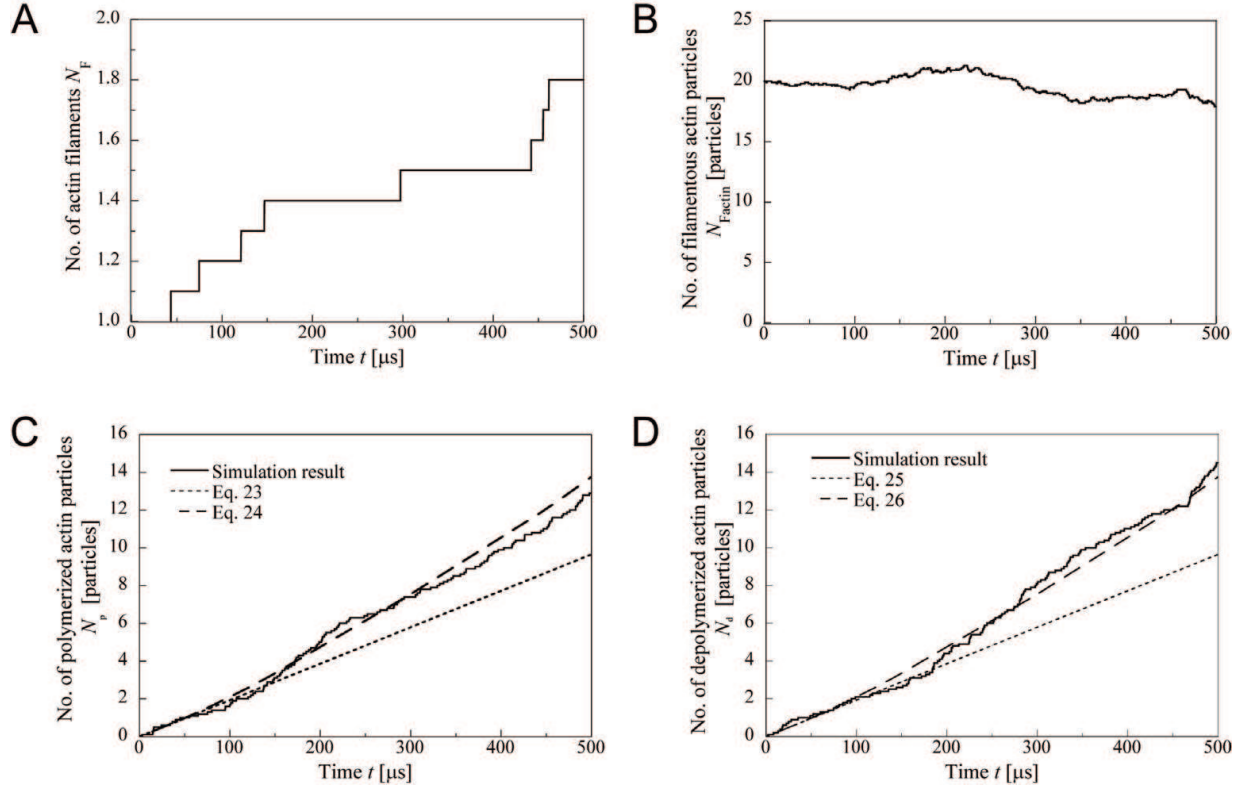


Figure 10: Change in number of filaments and particles in time. (A) Change in average number of filament N_F , (B) Change in average number of filamentous actin particles N_{Factin} , (C) Change in number of polymerized particles in time, and (D) Change in number of depolymerized particles in time.

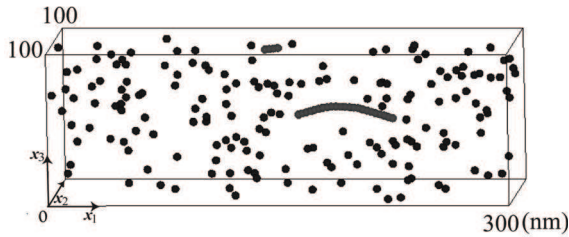


Figure 9: Snapshot of the filament under the fluctuations in severing simulation at $t = 500\mu s$.

trated in Fig. 10B, the polymerized actin particles N_p can be expressed as

$$\begin{aligned} N_p(t) &= \int_0^t N_F(\tau)k_p d\tau \\ &= \int_0^t \{N_F(\tau) \times 1.93 \times 10^{-2}\} d\tau, \quad (24) \\ N_p(0) &= 0, \end{aligned}$$

which is plotted by the dashed line in Fig. 10C. A

comparison of the dotted line in Eq. 23 with the dashed line in Eq. 24 shows that their gradients match each other in the beginning, and then, the dashed line becomes larger than the dotted line in time. This trend can be explained as follows: the increase in the number of the filament barbed ends due to severing, as shown in Fig. 2, causes the acceleration of the apparent actin filament elongation rate and polymerization (38, 39). Because the solid line (simulated result) agrees well with the dashed line in Eq. 24 in Fig. 10C, the change in the number of polymerized particles in time by severing was reproduced in this simulation.

In Fig. 10D, a change in the number of depolymerized actin particles N_d is shown. The solid line indicates the results in this simulation, and the dotted line indicates the following relation:

$$N_d(t) = k_d t = 1.93 \times 10^{-2} t, \quad (25)$$

which was obtained under the assumption of no

severing. The dashed line indicates the relation given by the equation,

$$\begin{aligned} N_d(t) &= \int_0^t N_F(\tau) k_d d\tau \\ &= \int_0^t \{N_F(\tau) \times 1.93 \times 10^{-2}\} d\tau, \quad N_d(0) = 0, \end{aligned} \quad (26)$$

which was obtained by considering the change in the number of filaments. A comparison of the dotted line in Eq. 25 with the dashed line in Eq. 26 shows that depolymerization is accelerated by an increase in the number of filament pointed ends as the number of filaments increases (10, 40). Because the solid line obtained in the simulation agrees well with the dashed line in Eq. 26 in Fig. 10D, the change in the number of depolymerized particles in time by severing was reproduced.

5 Discussion

In this study, we developed the mathematical model of actin filament dynamics, which can describe phenomena in the scale ranging from the dynamics of one molecule to the filament structural changes. Then, we simulated the actin filament dynamics to analyze filament elongation rate, filament turnover, and the effects of severing on polymerization/depolymerization. The results indicated that the model reproduced the linear dependence of filament elongation on time, filament turnover process by polymerization/depolymerization, and acceleration of polymerization/depolymerization by filament severing. And, even though the coupling of these filament dynamics phenomena was not directly formulated, the simulations naturally involved the coupling effects. Our results qualitatively agreed with those obtained in the experiments. Thus, the developed model could be the basis of the model that describes the actin filament dynamics from the molecular-level behavior.

The mechanical behaviors of the actin filament on various scales have been investigated through modeling and simulation. For example, on the cell migration scale, the relationship between actin filament dynamics and cell migration has been captured numerically using a finite element method

based on the model that combines actin dynamics, attachment, and retraction (31). On the filament structural changes scale, the distribution of actin filament length under the effects of polymerization/depolymerization and severing has been investigated using kinetic equations for the actin filament dynamics (25). On the scale ranging from the atomistic structural dynamics to filament structural changes, the barbed-pointed ends asymmetry of polymerization has been investigated by the Brownian dynamics method derived from atomistic structures (7). In this study, we focused on the scales ranging from the dynamics of actin molecules to filament structural changes, and developed new model for the actin filament dynamics. This model can be used to calculate the change in the number of polymerized/depolymerized actin molecules during actin filament dynamics. And, because its mechanical properties are modeled, actin filament deformation due to the random and external forces also can be calculated.

Having developed the model of actin filament dynamics for an isolated single actin filament in the scale ranging from the dynamics of a molecule to filament structural changes, it would be possible to extend to the higher-order structures formed by bundling and crosslinking (41, 42). In addition, by regulating the dynamics of actin-related proteins as well as actin particles using the Langevin equation with consideration of their interactions, the mechano-biochemical coupling model of actin filament dynamics could be developed. Furthermore, the developed model can be applied generally to the analysis of biological filamentous polymers such as microtubules (43, 44) and DNA (45).

In developing the model, we have made some assumptions and set some parameters empirically. For example, the polymerization distance Δ_p was set without considering the actin molecular polarity. The depolymerization and severing rates were set to be approximately 10^4 and 10^7 times larger than the experimental results (6, 46), respectively, to accelerate depolymerization and severing to fit the calculation time of 500 μ s. To avoid the numerical instability and to trace a phenomenon over a long time period, the spring constants,

K_{tensile} and K_{bend} , were reduced to 1/20 of the experimentally obtained results. The external force acting on the particles was based on the repulsive potential in Eq. 16, assuming the diffusion-limited reaction of the actin filament dynamics. Moreover, depolymerization and severing, which are regulated by interactions with biochemical factors such as profilin, cofilin, and Arp2/3 complex (47, 48), were modeled phenomenologically. Even though the above assumptions were used, the model could qualitatively reproduce basic characteristics such as the linearity of filament elongation, turnover process, and severing effects on the polymerization/depolymerization rates.

To describe actin filament dynamics in more detail, our next challenge will be modeling the filament nucleation, annealing, branching, bundling, and crosslinking. In addition, by taking into account biochemical factors such as profilin, cofilin, and Arp2/3 complex, we will be able to investigate their effects on the actin filament dynamics. Furthermore, in combination with the models for membrane dynamics and cell-substrate adhesion, it would be possible to investigate cellular functional activities (49, 50) such as shape changing, cell division, and migration, from molecular-level dynamics, using coarse graining modeling techniques.

Thus, focusing on the scales ranging from the dynamics of the molecules to the polymer structural changes using the Brownian dynamics simulation would enable us to gain new ideas to contribute to the research field of molecular and cellular biomechanics.

Acknowledgement: This work was partly supported by the Grant-in-Aid for Scientific Research from the Ministry of Education, Culture, Sports, Science and Technology of Japan, and by the 21st Century COE Program for Research and Education on Complex Functional Mechanical System at Kyoto University. We thank Dr. Hidetaka Yamaoka at RIKEN for his helpful suggestions on this study.

References

1. Pollard, T.D. & Borisy, G.G. (2003) *Cell*, 112, 453-465.
2. Sato, K., Adachi, T., Shirai, Y., Saito, N., & Tomita, Y. (2006) *J. Biomech. Sci. Eng.*, 1, 204-214.
3. Guilak, F. (1995) *J. Biomech.*, 28, 1529-1541.
4. Pollard, T.D., Blanchoin, L., & Mullins, R.D. (2000) *Annu. Rev. Biophys. Biomol. Struct.*, 29, 545-576.
5. Sato, K., Adachi, T., Matsuo, M., & Tomita, Y. (2005) *J. Biomech.*, 38, 1895-1901.
6. Pollard, T.D. (1986) *J. Cell Biol.*, 103, 2747-2754.
7. Sept, D., Elcock, A.H., & McCammon, J.A. (1999) *J. Mol. Biol.*, 294, 1181-1189.
8. Kobiela, A., Pasolli, H.A., & Fuchs, E. (2004) *Nat. Cell Biol.*, 6, 21-31.
9. Yamaguchi, H., Miki, H., Suetsugu, S., Ma, L., Kirschner, M.W., & Takenawa, T. (2000) *Proc. Natl. Acad. Sci. USA*, 97, 12631-12636.
10. Moriyama, K. & Yahara, I. (1999) *Embo J.*, 18, 6752-6761.
11. Furukawa, K., Fu, W.M., Li, Y., Witke, W., Kwiatkowski, D.J., & Mattson, M.P. (1997) *J. Neurosci.*, 17, 8178-8186.
12. Narumiya, S. & Mabuchi, I. (2002) *Nature*, 419, 27-28.
13. Chu, J.W. & Voth, G.A. (2005) *Proc. Natl. Acad. Sci. USA*, 102, 13111-13116.
14. Peskin, C.S., Odell, G.M., & Oster, G.F. (1993) *Biophys. J.*, 65, 316-324.
15. Carlsson, A.E. (2006) *Biophys. J.*, 90, 413-422.
16. Mogilner, A. & Oster, G. (1996) *Biophys. J.*, 71, 3030-3045.

17. Zigmond, S.H. (1993) *Cell Motil. Cytoskeleton*, 25, 309-316.
18. Chu, J.W. & Voth, G.A. (2006) *Biophys. J.*, 90, 1572-1582.
19. Ming, D.M., Kong, Y.F., Wu, Y.H., & Ma, J.P. (2003) *Biophys. J.*, 85, 27-35.
20. Mogilner, A. & Edelstein-Keshet, L. (2002) *Biophys. J.*, 83, 1237-1258.
21. Bossis, G., Quentrec, B., & Boon, J.P. (1982) *Mol. Phys.*, 45, 191-196.
22. Ermak, D.L. & McCammon, J.A. (1978) *J. Chem. Phys.*, 69, 1352-1360.
23. Hill, T.L. & Kirschner, M.W. (1982) *Proc. Natl. Acad. Sci. USA*, 79, 490-494.
24. Sept, D., Xu, J.Y., Pollard, T.D., & McCammon, J.A. (1999) *Biophys. J.*, 77, 2911-2919.
25. Edelstein-Keshet, L. & Ermentrout, G.B. (1998) *Bull. Math. Biol.*, 60, 449-475.
26. Drenckhahn, D. & Pollard, T.D. (1986) *J. Biol. Chem.*, 261, 2754-2758.
27. Elzinga, M., Collins, J.H., Kuehl, W.M., & Adelstein, R.S. (1973) *Proc. Natl. Acad. Sci. USA*, 70, 2687-2691.
28. Box, G.E.P. & Muller, M.E. (1958) *Ann. Math. Stat.*, 29, 610-611.
29. Mogilner, A. & Rubinstein, B. (2005) *Biophys. J.*, 89, 782-795.
30. McGrath, J.L., Osborn, E.A., Tardy, Y.S., Dewey, C.F., & Hartwig, J.H. (2000) *Proc. Natl. Acad. Sci. USA*, 97, 6532-6537.
31. Rubinstein, B., Jacobson, K., & Mogilner, A. (2005) *Multiscale Model. Sim.*, 3, 413-439.
32. Kojima, H., Ishijima, A., & Yanagida, T. (1994) *Proc. Natl. Acad. Sci. USA*, 91, 12962-12966.
33. Oosawa, F. (1980) *Biophys. Chem.*, 11, 443-446.
34. Yanagida, T., Nakase, M., Nishiyama, K., & Oosawa, F. (1984) *Nature*, 307, 58-60.
35. Mogilner, A. (2006) *Curr. Opin. Cell Biol.*, 18, 32-39.
36. Wegner, A. (1976) *J. Mol. Biol.*, 108, 139-150.
37. Gallo, G., Yee, H.F., & Letourneau, P.C. (2002) *J. Cell Biol.*, 158, 1219-1228.
38. Hartwig, J.H., Bokoch, G.M., Carpenter, C.L., Janmey, P.A., Taylor, L.A., Toker, A., & Stossel, T.P. (1995) *Cell*, 82, 643-653.
39. Barkalow, K., Witke, W., Kwiatkowski, D.J., & Hartwig, J.H. (1996) *J. Cell Biol.*, 134, 389-399.
40. Carlier, M.F., Laurent, V., Santolini, J., Melki, R., Didry, D., Xia, G.X., Hong, Y., Chua, N.H., & Pantaloni, D. (1997) *J. Cell Biol.*, 136, 1307-1322.
41. Winder, S.J. & Ayscough, K.R. (2005). *J. Cell Sci.*, 118, 651-654.
42. Deguchi, S., Ohashi, T., & Sato, M. (2005) *Mol. Cell. Biomech.*, 2, 205-216.
43. Desai, A. & Mitchison, T.J. (1997) *Annu. Rev. Cell Dev. Biol.*, 13, 83-117.
44. Ingber, D.E., Prusty, D., Sun, Z.Q., Betensky, H., & Wang, N. (1995) *J. Biomech.*, 28, 1471-1484.
45. Seeman, N.C. (2003) *Nature*, 421, 427-431.
46. Andrianantoandro, E. & Pollard, T.D. (2006) *Mol. Cell*, 24, 13-23.
47. Pantaloni, D., Boujemaa, R., Didry, D., Gounon, P., & Carlier, M.F. (2000) *Nat. Cell Biol.*, 2, 385-391.
48. Loisel, T.P., Boujemaa, R., Pantaloni, D., & Carlier, M.F. (1999) *Nature*, 401, 613-616.
49. Adachi, T., Sato, K., & Tomita, Y. (2003) *Biomechan. Model Mechanobiol.*, 2, 73-82.
50. Trickey, W.R., Vail, T.P., & Guilak, F. (2004) *J. Orthop. Res.*, 22, 131-139.

